RESEARCH ARTICLE

National Science Review
6: 914–920, 2019
doi: 10.1093/nsr/nwz110
Advance access publication 6 August 2019

PHYSICS

Log-periodic quantum magneto-oscillations and discrete-scale invariance in topological material $HfTe_5$

Huichao Wang[1,2,†], Yanzhao Liu[1,†], Yongjie Liu[3], Chuanying Xi[4], Junfeng Wang[3], Jun Liu[5], Yong Wang[5], Liang Li[3], Shu Ping Lau[2], Mingliang Tian[4], Jiaqiang Yan[6], David Mandrus[6,7], Ji-Yan Dai[2,*], Haiwen Liu[8,*], Xincheng Xie[1,9,10,11] and Jian Wang[1,9,10,11,*]

[1]International Center for Quantum Materials, School of Physics, Peking University, Beijing 100871, China; [2]Department of Applied Physics, The Hong Kong Polytechnic University, Hong Kong, China; [3]Wuhan National High Magnetic Field Center, Huazhong University of Science and Technology, Wuhan 430074, China; [4]High Magnetic Field Laboratory, Chinese Academy of Sciences, Hefei 230031, China; [5]Center of Electron Microscopy, State Key Laboratory of Silicon Materials, School of Materials Science and Engineering, Zhejiang University, Hangzhou 310027, China; [6]Materials Science and Technology Division, Oak Ridge National Laboratory, Oak Ridge, TN 37831, USA; [7]Department of Materials Science and Engineering, University of Tennessee, Knoxville, TN 37996, USA; [8]Center for Advanced Quantum Studies, Department of Physics, Beijing Normal University, Beijing 100875, China; [9]Collaborative Innovation Center of Quantum Matter, Beijing 100871, China; [10]CAS Center for Excellence in Topological Quantum Computation, University of Chinese Academy of Sciences, Beijing 100190, China and [11]Beijing Academy of Quantum Information Sciences, Beijing 100193, China

*Corresponding authors.
E-mails: jianwangphysics@pku.edu.cn; haiwen.liu@bnu.edu.cn; jiyan.dai@polyu.edu.hk
†Equally contributed to this work.

Received 24 June 2019; **Revised** 28 July 2019; **Accepted** 28 July 2019

ABSTRACT

Discrete-scale invariance (DSI) is a phenomenon featuring intriguing log-periodicity that can be rarely observed in quantum systems. Here, we report the log-periodic quantum oscillations in the longitudinal magnetoresistivity (ρ_{xx}) and the Hall traces (ρ_{yx}) of $HfTe_5$ crystals, which reveal the DSI in the transport-coefficients matrix. The oscillations in ρ_{xx} and ρ_{yx} show the consistent log$B$-periodicity with a phase shift. The finding of the log$B$ oscillations in the Hall resistance supports the physical mechanism as a general quantum effect originating from the resonant scattering. Combined with theoretical simulations, we further clarify the origin of the log-periodic oscillations and the DSI in the topological materials. This work evidences the universality of the DSI in the Dirac materials and provides indispensable information for a full understanding of this novel phenomenon.

Keywords: log-periodic oscillations, discrete-scale invariance, topological materials, Dirac materials, magnetoresistance, Hall resistance

INTRODUCTION

Discrete-scale invariance (DSI) is a partial breaking of continuous-scale invariance where observables of the system obey the scale invariance only for a geometrical set of choices written in the form of λ^n, with λ being the scaling ratio [1]. With the violation of the classical continuous-scale symmetry, the DSI represents a scale anomaly and the characteristic signature of DSI, the intriguing log-periodicity, exists in rupture, growth processes, turbulence, finance and so on. The appearance of log-periodic structures indicates the characteristic length scales in a system, which is extremely interesting when it is fundamentally related to the underlying physical mechanism [1].

The scale anomaly DSI is of high general interest while it can be rarely observed in quantum systems experimentally [2]. For a long time, the DSI has only been confirmed in cold atom systems and generated tremendous interest [3–10]. Nowadays, the DSI behavior in Dirac materials has also attracted attention in several subfields of physics [11–16]. Especially, the magneto-transport measurements on topological material $ZrTe_5$ reveal a new type of magnetoresistance (MR) oscillations with peculiar log-periodicity and thus manifest the appearance of DSI in a solid-state system [14]. Such a peculiar DSI feature is considered to be universal in Dirac materials with Coulomb attraction [14], which may be closely related to the quasi-bound states formed by massless Dirac fermions and the long-pursued atomic-collapse phenomenon [14,15,17]. Thus, it is desirable to explore the log-periodic quantum oscillations and the DSI in other physical observables, such as the Hall trace, and the comparison of the DSI features in different transport coefficients may provide insights into the underlying mechanisms. As a sister compound of $ZrTe_5$, the topological material $HfTe_5$ provides a promising platform [18–32].

In this work, we reveal the universality of the peculiar log-periodic quantum oscillations and DSI phenomenon in Dirac materials by the magneto-

transport results of $HfTe_5$ crystals. The oscillations with log$B$-periodicity are demonstrated in the MR behavior, almost independently of the minor differences of the sample quality. More importantly, the log$B$-periodicity is also discovered in the Hall traces of the $HfTe_5$ crystals. In addition, we observe a phase shift in the oscillations of ρ_{xx} and ρ_{yx} with consistent period, justifying the log$B$-periodic oscillations originating from the resonant scattering around the Fermi energy. Moreover, we elaborate on the relation between the DSI and the log-periodic oscillations in both the longitudinal MR and the Hall resistance, and explain the origin of the log$B$-periodic oscillations and the phase shift between ρ_{xx} and ρ_{yx}. This work provides new insights towards further understanding of the log-periodic quantum oscillations and the DSI in solid-state systems.

RESULTS

Magnetoresistance behavior

Single crystals $HfTe_5$ in our work were grown via a self-Te-flux method as in the previous report [23]. The atomically high-resolution transmission-electron-microscopy image of one typical sample is shown in the inset of Fig. 1a, which manifests a high-quality nature. The resistivity-temperature (ρT) characteristic of $HfTe_5$ crystals down to 2 K is shown in Fig. 1a. With decreasing temperatures, the samples show first the metallic behavior above approximately 200 K and then a semiconducting-like upturn. As the temperature is further decreased, sample-dependent resistivity peaks are observed at temperatures T_p varying from 20 to 40 K. At even lower temperatures, the semiconducting-like upturn recovers in most samples. It is noted here that the resistivity peak in the crystals cannot be attributed to Lifshitz transition, since the Hall remains positive up to room temperature with no sign change [23].

Figure 1b shows the MR behavior at 2 K of different samples from the same batch when the magnetic field is perpendicular to the layer orientation (B//b axis). The MR follows a sharp cusp at around zero magnetic field and changes much more slowly at high magnetic fields. The MR ($R(H)/R(0)$) values show sample dependence with a range of 1500–5500% at 15 T. According to the non-linear Hall data of $HfTe_5$ crystals, we would attribute the various ρT behavior and MR effect to the competition of a semi-metallic Dirac band and a semiconducting band in the material [33]. For Sample 3 (s3), the Fermi level is very close to the Dirac point and thus the Fermi surface of the Dirac pocket is tiny. The dominated semiconducting band induces the upturn resistance at low temperatures and the MR effect is small. On the contrary, the Dirac band dominates in s4, which gives rise to the metallic ρT behavior at low temperatures down to 2 K and the larger MR effect in s4. For the other two samples (s1 and s2), they exhibit the intermediate properties as shown in Fig. 1a and b. Since the transition-metal pentatelluride system is extremely sensitive to the cell volume, the slight diversity of these transport properties could be attributed to the minor quality differences in the samples. A similar two-band model was proposed to interpret the mysterious peak in $ZrTe_5$ considering either Te deficiency or iodine contamination [34,35]. The model might give a unified explanation for the various observations of the Dirac or semiconducting property in $ZrTe_5$.

By performing the second derivative for the MR results in Fig. 1b, oscillations can be distinguished from the large MR background. The characteristic magnetic fields B_n of oscillating peaks (marked with index n) and dips (n-0.5) in the oscillations are approximately consistent for different $HfTe_5$ samples (Fig. 1c and Supplementary Fig. S1). By plotting logB_n vs. n in Fig. 1d, the index dependence for different samples can all be reproduced by a linear fitting, which reveals that peaks and dips appear periodically as a function of log$B$ in $HfTe_5$. We identify that these specific magnetic fields satisfy the law of $B_n = \lambda \cdot B_{n+1}$, where λ is a characteristic scale factor for the material. From the index plot in

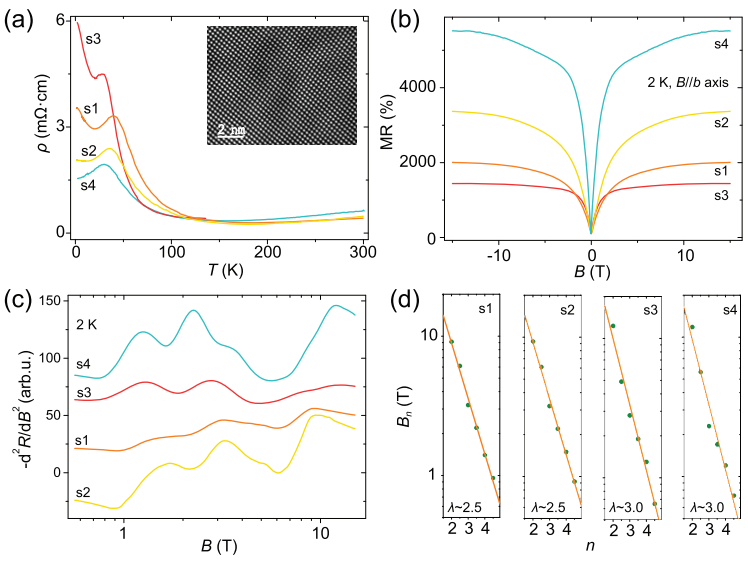

Figure 1. Resistivity-temperature characteristic and MR behavior of $HfTe_5$ single crystals. (a) Temperature dependence of the resistivity. Inset: the atomically high-resolution transmission-electron-microscopy image of $HfTe_5$ manifesting a high-quality nature. (b) MR at 2 K for $HfTe_5$ crystals in a perpendicular magnetic field. (c) The second derivative results of the MR behavior at 2 K shown in (b). Data curves are shifted for clarity. (d) Linear dependence of logB_n on the index n shows log-periodicity of the MR oscillations. B_n is the characteristic magnetic field for a peak or dip in the oscillations.

Fig. 1d, the dominant scale factor λ is shown to be 2.5 or 3.0.

The magneto-transport measurements at high magnetic fields up to 58 T further confirm the log*B*-periodic MR oscillations and DSI in $HfTe_5$ (Fig. 2 and Supplementary Fig. S2). For clarity, data curves in Fig. 2a and b are shifted. The pink curve for s5 in Fig. 2a is measured at a static magnetic field. The MR oscillations observed at lower magnetic fields can be well reproduced by the pulsed magnetic field measurements on s5 and more oscillations are observed at higher magnetic fields (orange and red), as guided by the dashed lines. Besides, the oscillations are also observed in other samples s6 and s7, where the resistance peaks and dips in s5 can be replicated. The oscillations can be extracted by subtracting a smooth background from the raw data in Fig. 2a and the results are shown in Fig. 2b. The consistent log*B*-periodicity can also be obtained by the second derivative of the raw MR data (see Supplementary Fig. S3). The index plots for the oscillations are shown in Fig. 2c, which confirms the log*B*-periodicity of the MR oscillations with more experimental points at ultrahigh magnetic fields (green dots). By performing the Fast Fourier Transform (FFT) of the log-periodic oscillations in Fig. 2b, a sharp FFT frequency peak is observed in various samples (Fig. 2d), which is consistent with the linear fitting results shown in Fig. 2c. It is worth noting that the factor λ has a broadening width in experiments. Based on an error bar determined by the full width at half maximum (FWHM) of the FFT frequency peak and combining with the results of different samples, we obtain a factor range of about [2.5, 5.9] in the $HfTe_5$ crystals.

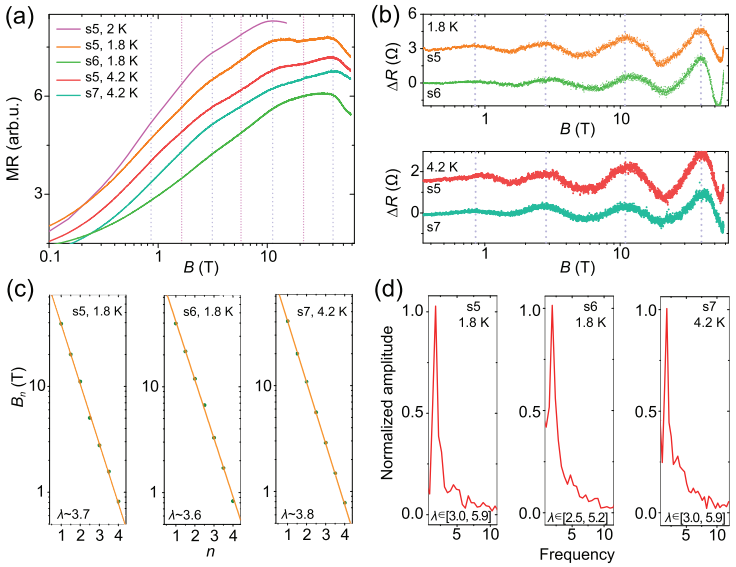

Figure 2. Log-periodic MR oscillations in $HfTe_5$. (a) MR of $HfTe_5$ vs. log*B*. The MR oscillations measured in PPMS (pink) is consistent with the results (orange and red) in the pulsed high magnetic field. MR oscillations are reproduced in different samples (s5, s6, s7). Dashed lines serve as guides to the eye. (b) Extracted MR oscillations from the raw data in (a) after subtracting a background. Data curves in (a) and (b) are shifted for clarity. (c) Log*B*-periodicity of the MR oscillations in $HfTe_5$. (d) FFT results of the MR oscillations in (b). Combining the results of different samples, the scale factor λ shows a range of about [2.5, 5.9] which is determined by the FWHM of the FFT frequency peak.

Temperature dependence

The temperature dependence of the log*B*-periodic oscillations in $HfTe_5$ is shown in Fig. 3. Figure 3a–c are results for s5 and Fig. 3d–f are results for another sample (s7). By subtracting background from the raw MR data in Fig. 3a and d, we obtain the oscillating resistance shown in Fig. 3b and e, respectively, and then perform FFT of the oscillations. The FFT amplitudes in Fig. 3c and f are normalized divided by the peak amplitude at the base temperature. Based on the theoretical formula of $A = A_0(1\text{-}\exp(-\Delta E/k_B T))$, the fitting of the FFT amplitude at varied temperatures gives a characteristic binding energy ΔE of 7.0 meV for s5 and 7.5 meV for s7. Here, ΔE refers to the binding energy of the states that induce log-periodic oscillations. It means that, when the energy is larger than this characteristic value, the states dissolve. The binding energies correspond to the disappearance temperatures of the oscillations equaling to 81 and 87 K for s5 and s7, respectively. The characteristic temperatures for both samples are consistent with our experimental observations.

Oscillations in Hall resistance

We finally investigated the influence of the DSI on the Hall traces of $HfTe_5$. In Fig. 4a, the Hall data of $HfTe_5$ clearly shows a non-linear dependence on the magnetic field, which is consistent with the two-band model. Distinct and consistent oscillations are observed in the Hall resistance of different samples. The second derivate results are shown in Fig. 4b. Similar to the property of oscillations on the MR, the characteristic log*B*-periodicity of the Hall resistance oscillations is confirmed by the linear index dependence (Fig. 4c). Here, the finding of the log*B* oscillations in the Hall resistance is quite meaningful, since it can identify the log*B* phenomenon in the total transport coefficients as a general quantum effect. We further compared the characteristic magnetic fields B_n where the peaks and valleys appear in the MR and the Hall resistance. Figure 4d and e shows the longitudinal MR (R_{xx}) and Hall results (R_{yx}) on the same sample (s11). The extracted oscillations from the R_{xx} and R_{yx} are shown in Fig. 4e.

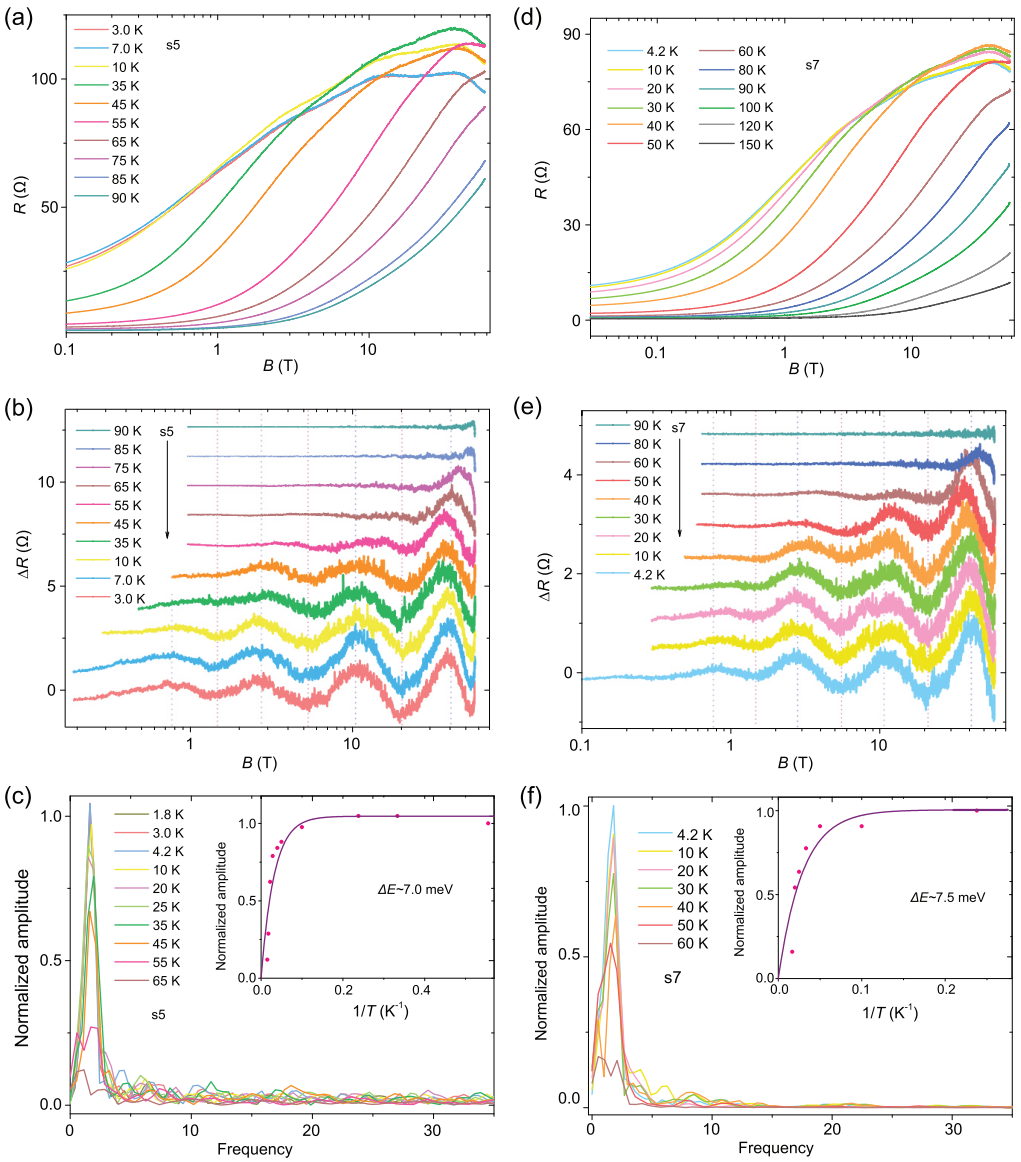

Figure 3. Temperature dependence of the log$B$-periodic oscillations. (a) MR of $HfTe_5$ (s5) at selected temperatures. (b) Log$B$-periodic oscillations in s5 at selected temperatures. (c) FFT results for the MR oscillations in (b). Inset: Theoretical fit on the normalized FFT amplitude at varying temperatures based on the theoretical formula $A = A_0(1\text{-}\exp(-\Delta E/k_B T))$. The fitted value is consistent with the experimental observations. (d)–(f) are results for another sample (s7). The fitting parameter is also consistent with experiments. The fitting results indicate that the disappearance temperature of the oscillations in the $HfTe_5$ crystal is about 80–90 K. Data curves in (b) and (e) are shifted for clarity.

The overlapped frequency peaks in Fig. 4f indicate the consistent log$B$-periodicity in the behavior of MR and Hall. Moreover, it is found that, in the oscillations, the phase of R_{yx} is slightly ahead of R_{xx}. The phase difference between R_{yx} and R_{xx} is reminiscent of that in the 2D quantum Hall effect [36]. Thus, the log-periodic quantum magneto-oscillations in both the longitudinal MR and the Hall traces indicate the underlying DSI property of the topological material $HfTe_5$ and its evolution under the magnetic field.

DISCUSSION

As discussed previously [14], the log-periodic quantum magneto-oscillations cannot be attributed to the conventional quantum oscillations, such as the Shubnikov–de Haas oscillations even with the consideration of the Zeeman effect. In addition, the peculiar phenomenon shows different features compared with the field-induced Fermi surface deformation or reconstruction scenario, such as the density-wave transition. It is suggested that log-periodic oscillations are closely related to the

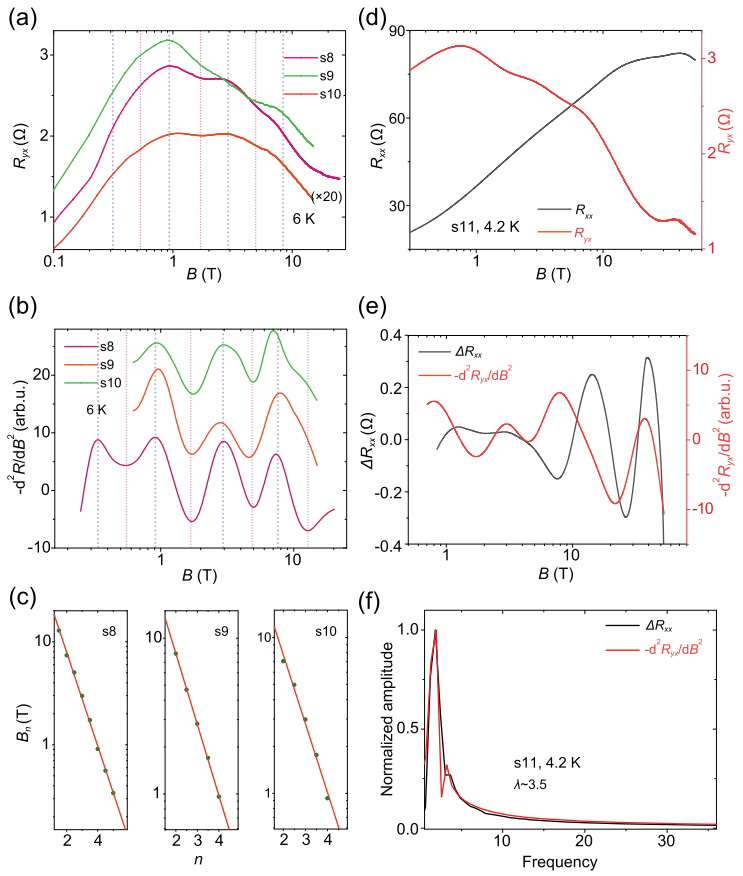

Figure 4. Signals of log$B$-periodic oscillations in the Hall traces of $HfTe_5$. (a) Hall traces of $HfTe_5$ crystals at 6 K versus the magnetic field. (b) The second derivative results of the curves in (a). Data curves are shifted for clarity. (c) The log-periodicity of the oscillating Hall resistance. (d) Comparison of R_{xx} and R_{yx} in the same sample (s11). (e) Comparison of the oscillations in R_{xx} and R_{yx} in the same sample s11. (f) FFT results for the oscillations in R_{xx} and R_{yx}.

quasi-bound states of Weyl particles from Coulomb attraction (see Supplementary Fig. S4) [14] and the resonant scattering between the mobile carriers and the quasi-bound states around the Fermi level determines the DSI features in both the longitudinal MR and the Hall traces.

The oscillation term in ρ_{xx} and ρ_{yx} can be obtained by the T-matrix approximation and the theoretical quantum magneto-oscillations curves in ρ_{xx} and ρ_{yx} are shown in Supplementary Fig. S5. We can see that both ρ_{xx} and ρ_{yx} satisfy the log-periodic property. Furthermore, the peaks of $\Delta\rho_{xx}$ correspond to the nodes of $\Delta\rho_{yx}$, indicating a $\pi/2$ phase shift in the oscillations of ρ_{xx} and ρ_{yx}. The theoretical formulas signify that the $\pi/2$ phase shift originates from the resonant scattering between the mobile carriers and the quasi-bound states, sharing the same origin of the log-periodic oscillations. The experimental observations of R_{xx} and R_{yx} reveal that the phase of R_{yx} is slightly ahead of R_{xx}, consistently with the theoretical simulations. Here, we point out that the oscillations can be qualitatively viewed as a density-of-states effect, which refers to increased density of states when the quasi-bound states evolve into the Fermi energy. However, the quantitative understanding of the DSI in ρ_{xx} and ρ_{yx} and their phase shift needs the introduction of scattering. Since the quasi-bound states cannot transfer charge, these quasi-bound states contribute to the transport property by scattering with mobile carriers when the quasi-bound states locate at the Fermi energy. Previously, the 2D quantum Hall effect [36] also shows the $\pi/2$ phase shift between ρ_{xx} and ρ_{yx} when changing the magnetic field, which can also be explained by the scattering mechanism.

The correction to ρ_{xx} is in the order n_C/n_S, while that to ρ_{yx} is in the order n_C/N; here, n_C, n_S and N denote the density of the quasi-bound states, the density of short-range impurity and the total carrier density, respectively. Thus, the log-periodic magneto-oscillations only occupy a small percentage of the total resistance due to the small ratio of n_C/n_S and n_C/N. In $HfTe_5$, the oscillating resistance is about 0.4–0.9% of the longitudinal MR for the $n = 2$ peak as shown in Fig. 3 and the oscillations in the Hall resistance are more apparent (about 2%) as shown in Fig. 4. When comparing the results of $HfTe_5$ with those of $ZrTe_5$ [14], we find two differences. First, the oscillating amplitude of the log-periodic quantum oscillations in ρ_{xx} of $HfTe_5$ is relatively smaller. We attribute the phenomenon to a large n_S and relatively small n_C/n_S; thus, the correction to ρ_{xx} is weak. Meanwhile, due to the relatively large impurity scattering from these short-range impurities, the broadening effect smears the log-periodic oscillations at small magnetic fields, ultimately leading to fewer observable oscillating cycles. Second, the log-periodicity in ρ_{yx} of $HfTe_5$ is relatively more remarkable. This feature may be due to the relatively large value for the density of charge impurity and thus relatively large value for the density of quasi-bound states n_C and the ratio n_C/N, which gives rise to considerable correction for Hall trace ρ_{yx} in $HfTe_5$.

Besides the consideration shown above, in real systems, other issues can influence the DSI property. First, both a small band gap Δ and finite screening length λ_S impose constraint on the DSI feature by introducing an effective low-energy cut-off. But the quasi-bound states with binding energy larger than the band gap Δ and radius smaller than λ_S cannot be influenced. Direct estimation gives the largest value of radius R_C and corresponding magnetic length $l_{B,C}$ satisfying $R_c \approx \sqrt{2\cdot s_0}\cdot l_{B,C} \approx \sqrt{2\cdot s_0}\cdot \min(\hbar v_F/\Delta, \lambda_s)$. Here $s_0 = \sqrt{(Z\cdot\alpha)^2 - 1}$, with Z denoting the number of the central charge and

α denoting the fine structure constant. If one sets Δ = 4 meV and neglects the screening effect, $R_C \approx 83$ nm and the corresponding magnetic field $B_C \approx 0.8$ T. Second, in the system with ultralow carrier density, both the charge impurity and the carrier from the electron band can generate the Coulomb attraction [16]. Here, λ is determined by $Z \cdot \alpha$, with $\lambda = e^{2\pi/s_0}$ [14]. The effective fine structure constant $\alpha = \frac{e^2}{4\pi\varepsilon_0\hbar v_F}$ depends on the Fermi velocity v_F in Dirac materials and is expected to be universal in one system irrelevant to mobility and carrier density. Moreover, the Coulomb attraction $V(\overrightarrow{R}) = \frac{-Ze^2}{4\pi\varepsilon_0 R}$ is determined by the central charge Ze, including the charge impurity or the carriers from the electron band. Indeed, λ shows a small difference in different samples (around 3.6, 3.7 and 3.8 for the three samples) and is almost independent of the minor differences in the sample quality, which indicates that the effective charge Ze is very close for different samples, and opposite type of carriers or similar charge impurities acting as the charge center. Third, the magnetic field significantly influences a certain n-th quasi-bound state when the magnetic length l_B satisfies the relation $R_n \approx \sqrt{2 \cdot s_0}\, l_B$ [14]. In $HfTe_5$, the oscillation peaks locate in the range [0.8 T, 40 T] and $s_0 \approx 4.8$; the corresponding radii of the quasi-bound states locate in the range of 90 $\sim$ 10 nm. Finally, a non-oscillating background is subtracted for magneto-oscillations in MR, which is commonly utilized in analysis of quantum oscillations [37,38] and does not influence the DSI feature in our investigations.

CONCLUSIONS

In summary, we report the intriguing log-periodic quantum magneto-oscillations in both the Hall and the MR results in the topological material $HfTe_5$, which indicate the underlying DSI feature in the system. The observation of the log-periodicity in both physical observables ρ_{xx} and ρ_{yx} reveals that the DSI shows an overall effect on the transport properties for a Dirac system with the long-range Coulomb attraction. In particular, the finding of the log$B$ oscillations in the Hall resistance suggests the general quantum-effect scenario. The origin of the DSI and its relation to the log-periodic magneto-oscillations are further elucidated theoretically. This work paves the way for further research on the log-periodic oscillations and the DSI in quantum systems.

METHODS

Single crystals of $HfTe_5$ in our work were grown via a self-Te-flux method. The crystals were chemically and structurally analysed by powder X-ray diffraction, scanning electron microscopy with energy-dispersive X-ray spectroscopy and transmission electron microscopy. Electrical transport measurements in this work were conducted in three systems: a 16 T- PPMS (Physical Property Measurement System) from Quantum Design, a pulsed high magnetic field facility (58 T) at Wuhan National High Magnetic Field Center and a static magnetic field up to 25 T in the High Magnetic Field Laboratory in Hefei. Results from different measurement systems and different samples are reproducible and consistent with each other. The standard four/six-electrode-method was used for the MR/Hall measurements with the excitation current flowing along the crystallographic a-axis of $HfTe_5$.

SUPPLEMENTARY DATA

Supplementary data are available at *NSR* online.

ACKNOWLEDGEMENTS

We acknowledge Haipeng Zhu, Jiezun Ke, Jun Ge and Zhibo Dang for their help in the work.

FUNDING

This work was financially supported by National Key Research and Development Program of China (2018YFA0305604, 2017YFA0303300, 2015CB921102, 2017YFA0304600), the National Natural Science Foundation of China (11888101, 11774008, 11674028, 11534001, 11504008), the Strategic Priority Research Program of Chinese Academy of Sciences (XDB28000000), the Beijing Natural Science Foundation (Z180010), the Fundamental Research Funds for the Central Universities, Hong Kong GRF Grant (153094/16P), the Hong Kong Polytechnic University Strategic Plan (1-ZE25 and 1-ZVCG) and the Postdoctoral Fellowships Scheme (1-YW0T). Work at ORNL was supported by the US Department of Energy, Office of Science, Basic Energy Sciences, Division of Materials Sciences and Engineering.

REFERENCES

1. Sornette D. Discrete-scale invariance and complex dimensions. *Phy Rep* 1998; **297**: 239–70.
2. Landau LD and Lifshitz EM. *Quantum Mechanics: Non-relativistic Theory*, 3rd edn. Oxford: Perganon Press, 1977.
3. Efimov V. Energy levels arising from resonant two-body forces in a three-body system. *Phys Lett B* 1970; **33**: 563–4.
4. Braaten E and Hammer HW. Universality in few-body systems with large scattering length. *Phys Rep* 2006; **428**: 259–390.
5. Naidon P and Endo S. Efimov physics: a review. *Rep Prog Phys* 2017; **80**: 056001.
6. Kraemer T, Mark M and Waldburger P *et al*. Evidence for Efimov quantum states in an ultracold gas of caesium atoms. *Nature* 2006; **440**: 315–8.

7. Huang B, Sidorenkov LA and Grimm R *et al*. Observation of the second triatomic resonance in Efimov's scenario. *Phys Rev Lett* 2014; **112**: 190401.
8. Pires R, Ulmanis J and Häfner S *et al*. Observation of Efimov resonances in a mixture with extreme mass imbalance. *Phys Rev Lett* 2014; **112**: 250404.
9. Tung SK, Jimenez-Garcia K and Johansen J *et al*. Geometric scaling of Efimov states in a ^{6}Li-^{133}Cs mixture. *Phys Rev Lett* 2014; **113**: 240402.
10. Kunitski M, Zeller S and Voigtsberger J *et al*. Observation of the Efimov state of the helium trimer. *Science* 2015; **348**: 551–5.
11. Greiner W, Muller B and Rafelski J. *Quantum Electrodynamics of Strong Fields*. Berlin: Springer-Verlag, 1985.
12. Shytov AV, Katsnelson MI and Levitov LS. Atomic collapse and quasi–Rydberg states in graphene. *Phys Rev Lett* 2007; **99**: 246802.
13. Nishida Y. Vacuum polarization of graphene with a supercritical coulomb impurity: low-energy universality and discrete scale invariance. *Phys Rev B* 2014; **90**: 165414.
14. Wang H, Liu H and Li Y *et al*. Discovery of log-periodic oscillations in ultra-quantum topological materials. *Sci Adv* 2018; **4**: eaau5096.
15. Ovdat O, Mao J and Jiang Y *et al*. Observing a scale anomaly and a universal quantum phase transition in graphene. *Nat Commun* 2017; **8**: 507.
16. Zhang P and Zhai H. Efimov effect in the Dirac semi-metals. *Front Phys* 2018; **13**: 137204.
17. Wang Y, Wong D and Shytov AV *et al*. Observing atomic collapse resonances in artificial nuclei on graphene. *Science* 2013; **340**: 734–7.
18. Furuseth S, Brattas L and Kjekshus A. Crystal structure of $HfTe_5$. *Acta Chem Scand* 1973; **27**: 2367–74.
19. Izumi M, Uchinokura K and Matsuura E. Anomalous electrical resistivity in $HfTe_5$. *Solid State Commun* 1981; **37**:641–2.
20. Kamm GN, Gillespie DJ and Ehrlich AC *et al*. Fermi surface, effective masses, and energy bands of $HfTe_5$ as derived from the Shubnikov–de Haas effect. *Phys Rev B* 1987; **35**: 1223.
21. Tritt TM, Lowhorn ND and Littleton RT *et al*. Large enhancement of the resistive anomaly in the pentatelluride materials $HfTe_5$ and $ZrTe_5$ with applied magnetic field. *Phys Rev B* 1999; **60**:7816.
22. Weng H, Dai X and Fang Z. Transition-metal pentatelluride $ZrTe_5$ and $HfTe_5$: a paradigm for large-gap quantum spin hall insulators. *Phys Rev X* 2014; **4**: 011002.
23. Wang H, Li CK and Liu H *et al*. Chiral anomaly and ultrahigh mobility in crystalline $HfTe_5$. *Phys Rev B* 2016; **93**: 165127.
24. Zhao LX, Huang XC and Long YJ *et al*. Anomalous magneto-transport behavior in transition metal Pentatelluride $HfTe_5$. *Chin Phys Lett* 2017; **34**: 037102.
25. Son DT and Spivak BZ. Chiral anomaly and classical negative magnetoresistance of Weyl metals. *Phys Rev B* 2013; **88**: 104412.
26. Burkov AA. Chiral anomaly and transport in Weyl metals. *J Phys Condens Matter* 2015; **27**: 113201.
27. Wang J, Li H and Chang C *et al*. Anomalous anisotropic magnetoresistance in topological insulator films. *Nano Res* 2012; **5**: 739–46.
28. Dai X, Du ZZ and Lu HZ. Negative magnetoresistance without chiral anomaly in topological insulators. *Phys Rev Lett* 2017; **119**: 166601.
29. Qi Y, Shi W and Naumov PG *et al*. Pressure-driven superconductivity in the transition-metal pentatelluride $HfTe_5$. *Phys Rev B* 2016; **94**: 054517.
30. Liu Y, Long YJ and Zhao LX *et al*. Superconductivity in $HfTe_5$ across weak to strong topological insulator transition induced via pressures. *Sci Rep* 2017; **7**: 44367.
31. Fan Z, Liang QF and Chen YB *et al*. Transition between strong and weak topological insulator in $ZrTe_5$ and $HfTe_5$. *Sci Rep* 2017; **7**: 45667.
32. Zhang Y, Wang C and Liu G *et al*. Temperature-induced Lifshitz transition in topological insulator candidate $HfTe_5$. *Sci Bull* 2017; **62**: 950–6.
33. Niu J, Wang J and He Z *et al*. Electrical transport in nanothick $ZrTe_5$ sheets: from three to two dimensions. *Phys Rev B* 2017; **95**: 035420.
34. Shahi P, Singh DJ and Sun JP *et al*. Bipolar conduction is the origin of the electronic transition in pentatellurides: metallic vs. semiconducting behavior. *Phys Rev X* 2018; **8**: 021055.
35. Miller SA, Witting I and Aydemir U *et al*. Polycrystalline $ZrTe_5$ parametrized as a narrow-band-gap semiconductor for thermoelectric performance. *Phys Rev Appl* 2018; **9**: 014025.
36. Wei HP, Tsui DC and Pruisken AMM. Localization and scaling in the quantum hall regime. *Phys Rev B* 1986; **33**: 1488(R).
37. Schoenberg D. *Magnetic Oscillations in Metals*. Cambridge: Cambridge University Press, 1984.
38. Zhang C, Ni Z and Zhang J *et al*. Ultrahigh conductivity in Weyl semimetal NbAs nanobelts. *Nat Mater* 2019; **18**: 482–8.